Journal of Physics D: Applied Physics

PAPER

Etching mechanisms of graphene nanoribbons in downstream H_2 plasmas: insights from molecular dynamics simulations

To cite this article: A Davydova *et al* 2015 *J. Phys. D: Appl. Phys.* **48** 195202

Etching mechanisms of graphene nanoribbons in downstream H_2 plasmas: Insights from molecular dynamics simulations

A. Davydova[1], E. Despiau-Pujo[1,a)] G. Cunge[1] and D.B. Graves[2]

[1]*Univ. Grenoble Alpes, CNRS, CEA-Leti Minatec, LTM, F-38054 Grenoble Cedex*

[2]*Department of Chemical & Biomolecular Engineering, University of California at Berkeley, Berkeley, CA 94720, USA*

ABSTRACT

Lateral etching mechanisms of graphene nanoribbons (GNR) with zigzag (ZZ) edges in downstream H_2 plasmas are investigated using Molecular Dynamics simulations. A new etching mechanism is found, which occurs in three consecutive phases and requires a continuous exposure of GNRs to H atoms and high substrate temperatures (~800K). Full hydrogenation of GNR free edges during Phase 1 reduces the potential barriers to H chemisorption on near-edge C atoms from the basal plane. Subsequent hydrogenation of near-edge C-C dimers creates mechanical stress between C atoms (due to local sp^2-to-sp^3 rehybridizations) which leads to the rupture of C-C dimers bonds, unzipping locally the 1st and 2nd edge carbon rows. The unzipping then propagates randomly along the GNR edges and creates suspended linear carbon chains (Phase 2). Weakened by their exposure to continuous H bombardment and strong thermal vibrations, the suspended carbon chains may then rupture, leading to the sputtering of their carbon atoms as single C atoms or C_2 molecules (Phase 3). Thus no formation of volatile hydrocarbon etching products is observed in this 3-phase mechanism, which explains why the ribbon edges can be sharp-cut without generation of line-edge roughness, as also observed experimentally. Influence of substrate temperature on ZZ-GNRs etching is investigated and suggests the dominant mechanisms for understanding the temperature dependence of the etch rate observed experimentally (peaks at 800K and decreases for lower or higher temperatures).

a) Author to whom correspondence should be addressed. Electronic mail: emilie.despiau-pujo@cea.fr

I. INTRODUCTION

Due to the unique physico-chemical properties arising from its 2D planar structure, graphene has recently attracted considerable scientific and technological interest[1-4]. This material exhibits great potential for promising applications in many fields including nanoelectronics, where graphene has been proposed to replace silicon for the fabrication of next-generation electronic devices such as high-speed transistors[2]. However, electronic applications are handicapped by the absence of a semiconducting gap in pristine graphene. Bandgap engineering of graphene is thus an important challenge for the development of graphene-based nanoelectronic devices[5-6]. Different approaches have been tried to open sizeable and well-tuned bandgaps in single and bi-layer graphene - including chemical functionalization by hydrogenation[7-9] or fluorination[10-11], as well as boron and nitrogen substitutional doping[12] - but no mature process has been developed yet. Alternatively, a bandgap can also be obtained through quantum confinement by patterning graphene nanoribbons (GNRs) with sub-5 nm width and well controlled edges[13-14]. Due to their reduced dimensions and active electronic edge states, GNRs can indeed exhibit finite (non-zero) bandgap values, the bandgap magnitude being approximately inversely proportional to the nanoribbon width[14]. However, since the electronic structure of GNRs is extremely sensitive to their lateral dimension, controlled GNRs synthesis demands near-perfect edge engineering with no line edge roughness (LER) formation.

For practical applications, nanoribbons with widths of ~2-5 nm should be patterned. This can be achieved using bottom-up methods[15], however such techniques are usually not well adapted to large-area wafers.[16] Another solution is to use a top-down approach, in which the graphene is patterned using a combination of photolithography and plasma etching techniques. Several groups have used this method to synthesise GNRs[17,18] and fabricate first single-electron[19] and field-effect[20] graphene-based transistors. However, this combined method is limited by the

lithographic mask resolution and the line width roughness (LWR). For instance, for electron-beam lithography, the etch pattern resolution is generally restricted to a critical dimension ~10 nm with a LWR ~3nm. Although solutions may be found using high resolution alternative lithography techniques such as self-assembled block-copolymer etch masks,[21] it remains possible to reach sub-10 nm nanoribbons dimensions with lower resolution lithography by using a two-step process.[22-25] In the first step, the top-down approach is used to pattern >10 nm-width graphene nanoribbons. To do so, the graphene sample is usually etched through an e-beam patterned photoresist mask by H_2 or O_2 plasmas. In a second step, the lateral dimension of the GNR is reduced to the desired size, i.e., it is etched laterally (or trimmed) without damaging its surface. This second/lateral etching step is a challenging task since the properties of GNRs depend strongly on their width, as well as on the crystallographic orientation and the atomic structure of their edges.

Several methods have recently been explored to trim GNRs based on dry etching techniques. Wang and Dai reported a gas-phase etching procedure (without plasma) at high-temperature (800°C) in $NH_3/O_2/Ar$ mixtures, which allowed to narrow 20 nm-wide GNRs (obtained from lithographic patterning) down to 8 nm without damaging their basal plane, as evidenced by Raman spectroscopy[23]. However, this over-etching/trimming step resulted in breaks along the ribbons due to the edge roughness and width variations in the as-patterned GNRs after the lithographic patterning step[23]. Diankov et al.[24] studied the influence of remote hydrogen plasmas on graphene deposited on SiO_2 or mica substrates. They showed that etching was highly anisotropic and proceeded from the sheet edges or from pre-existing defects, with an etch rate displaying a pronounced dependence on the sample temperature: very slow at room temperature, peaking around 400°C and suppressed entirely at 700°C[24]. Other recent studies indicated that GNRs trimming could be achieved by using downstream H_2 plasmas, in which H atoms attack

preferentially the edges of the ribbons. Xie et al.[25] reported selective etching of GNRs edges (without damaging the basal plane) in a remote hydrogen plasma system, at 300 mTorr and for a substrate temperature of 300°C. Anisotropic etching of graphene by H_2 plasmas was also observed by Yang et al. in a remote inductively coupled plasma (ICP) system[22]. They report that the RF power and the substrate temperature T_s were the key parameters to control the lateral etching rate of monolayer and bilayer graphene. For a constant 50W RF power, the lateral etching rate was shown to increase with the substrate temperature until T_s=450°C (where it reaches a local maximum of 8 nm/min) and to then decrease close to zero values at T_s=700°C[22].

In the above experimental studies, the distance between the graphene/GNR samples and the plasma source was large (~40 cm) to avoid exposing the graphene surface to energetic ions. It means that mostly H plasma radicals could reach the graphene sample and participate in its etching. No further studies were carried out to understand the etching mechanism itself but the authors proposed a mechanism involving two steps: (i) the hydrogenation of C atoms at the edges by reactive H species of the plasma to form C-H groups followed by (ii) the breaking/cleavage of adjacent C-C bonds with the release/formation of CH_4 etch by-products[22,24,25]. These conclusions were made based on reaction mechanisms usually observed in plasma etching processes but were not confirmed experimentally in the case of graphene etching; i.e. the formation of methane etching products was not detected by any diagnostics. In particular, it still remains unclear how H radicals can selectively react with graphene edges without etching or introducing defects in its basal plane, and without creating line edge roughness. Indeed, one would expect the H attack of C at graphene edges to form CH_4 to be a random chemical process, which would inevitably lead to the generation and propagation of roughness on the edges. However experiments report that GNRs at the zigzag edges (not the armchair edges) were etched in a self-limiting manner, which suggests that a different etching mechanism may be involved here.

Hence, in this paper, we perform Molecular Dynamics (MD) simulations of hydrogen/GNRs interaction in downstream H_2 plasmas to investigate the lateral etching mechanism of suspended zigzag (ZZ) GNRs. Atomistic methods are a natural tool to study such problems since they provide insights into the physico-chemical reactions at the atomic scale. Because the experimental etch rate was shown to depend strongly on the sample temperature - very slow at 300°C (~570K), peaking around 450°C (~730K) and suppressed almost entirely at 700°C (~970K)[22,24] - we investigated numerically a broad temperature range. MD simulations were run at 300K, 600K, 800K and 1000K. Since the highest etch rate was found numerically at 800K (close to the experimental peak value of ~730K), this paper focuses on the fundamental understanding of the etch mechanism of ZZ-GNRs at 800K. It also provides elements explaining why the GNRs etch rate may depend on the substrate temperature (peaks at 800K and decreases for lower or higher substrate temperatures). The article is organized as follows. Section II describes important characteristics of the computational method used to study the interaction between H radicals and suspended ZZ-GNRs. Section III presents and discusses results about the 3 phases (edge carbons hydrogenation, unzipping and sputtering) of the etching mechanism at 800K and the substrate temperature influence on this process. Our conclusions are given in section IV.

II. COMPUTATIONAL METHODS

Classical Molecular Dynamics (MD) refers to a class of simulations that solve Newton's equations of motion for a system of interacting particles, treating each atom as a classical point and modeling the quantum effects from electrons by an interatomic potential energy function. This semi-empirical function describes the potential energy surface that results from an instantaneous configuration and attempts to model the forces between atoms, as well as changes

in covalent bonding.[26] In this work, the 2nd generation C-H REBO potential developed by Brenner and coworkers[27] is used to study the interactions between H radicals and ZZ-GNRs. This potential – widely used to model solid carbon and hydrocarbon systems – was successfully tested against DFT calculations to study elementary processes of graphene-hydrogen interaction in a former paper[28]. As shown in figure 1, the initial configuration is a suspended 2nm-wide single-layer GNR (L_x=41Å, L_y=19Å) which contains 340 carbon atoms with a surface area ~780Å^2. Periodic boundary conditions are imposed along the Ox axis only in order to mimic a semi-infinite ribbon with free zigzag edges. Two carbon atoms are maintained fixed on the periodic edges to anchor the graphene surface during cumulative hydrogen bombardment. The GNR is then quenched at various surface temperatures T_S (300K, 600K, 800K, 1000K) using the Berendsen thermostat[29], before being exposed to an isotropic flux of hydrogen thermal radicals. To model physically realistic conditions, we assumed that the H radicals' temperature is close to the surface/substrate temperature, a reasonable first approximation for a flowing downstream plasma system in contact with a heated substrate. Therefore the radicals' impacting kinetic energy E_R is sampled from a Maxwell-Boltzmann energy distribution at temperature T_S. For all impact trajectories, simulations are performed in the microcanonical (NVE) ensemble. The numerical integration scheme used to compute positions and velocities is the velocity-Verlet algorithm[30] with a timestep of 5x10^{-3} fs. Due the relative lightness of hydrogen and the appearance of numerical instability of graphene free edges at high surface temperatures, the timestep has to be strongly reduced (compared to previous plasma-surface simulations) to prevent unphysical events arising from numerical integration artefacts.

The simulations performed in this paper are similar in form to those described in previous papers[31,32]. The isotropic H bombardment of GNRs is simulated by impacting the surface at random locations and with random H directions. After each H impact, the motion of all

atoms is followed during a few tenths of picoseconds to capture the physics of the interaction (H reflection, C-H bond formation, etch product formation, etc.). Simulation of continuous H exposure is performed as a set of recursive impact trajectories, where the output configuration for impact *i* is used as the input configuration for impact *i+1*. For any realistic downstream discharge, radical fluxes are such that H atoms would impact the surface approximately once every 10^{-8}-10^{-6} s. Since simulation of the μs to ηs interval is not tractable with MD, events occurring in the relatively long times between impacts are not directly simulated. Instead, it is assumed that nothing happens during this time except for dissipation of eventual excess kinetic energy[31,32]. For this reason, simulation results are reported in terms of fluence (atoms/cm^2) rather than in flux or time. And in order to mimic the natural conduction of heat out of the cell, the Berendsen heat bath is applied to cool the cell back to its initial temperature T_S after each impact[29].

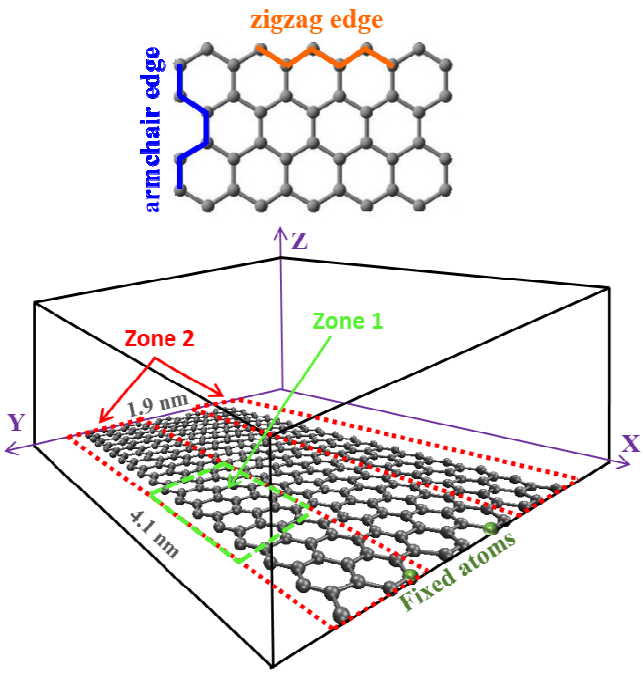

Figure 1. (top) Armchair (AC) and zigzag (ZZ) edges of graphene. (bottom) Simulation cell used in the MD calculation: GNR with free ZZ-edges with two fixed atoms and periodic boundaries applied along the Ox axis. Green (zone 1) and red (zone 2) zones indicate the restricted areas used for H cumulative bombardment of the surface.

As expected, preliminary simulations of isotropic H exposure of the full GNRs at various T_S showed only little modification of the surface after 5000 impacts (fluence ~$6x10^{16}$atom/cm^2): the basal plane was intact and only a few H atoms had bound on the free ZZ-edges. These calculations confirmed that the probability of surface modification was low because H radicals could only attack GNRs on edges due to the presence of potential barriers (~0.4-0.6 eV) on the basal plane arising from delocalized pi-electrons[28]. To accelerate the calculations (which would have taken several months in such conditions) and to focus on the etching mechanism, the zones for H bombardment were thus restricted to smaller areas. A small area – called zone 1 – centered on one free edge of the full GNR was selected to investigate the fundamental etching mechanisms of the ribbon at 800K and the surface temperature influence (green zone in figure 1). A larger area – called zone 2 – was selected to study the propagation of the etch front and the trimming of the full GNR at 800K (red zone in figure 1). In both cases, only the free edges and a few adjacent carbon rows from the basal plane are exposed to plasma radicals, i.e. those that are susceptible to react; the remainder of the cell is simulated but not bombarded. Such a choice allows to greatly reduce the computation time cost without information loss since a significant part of the basal plane remains bombarded by H radicals.

III. RESULTS AND DISCUSSION

A. Fundamental etching mechanisms of ZZ-GNRs

1. Lateral etching mechanism of ZZ-GNRs at T_S = 800K

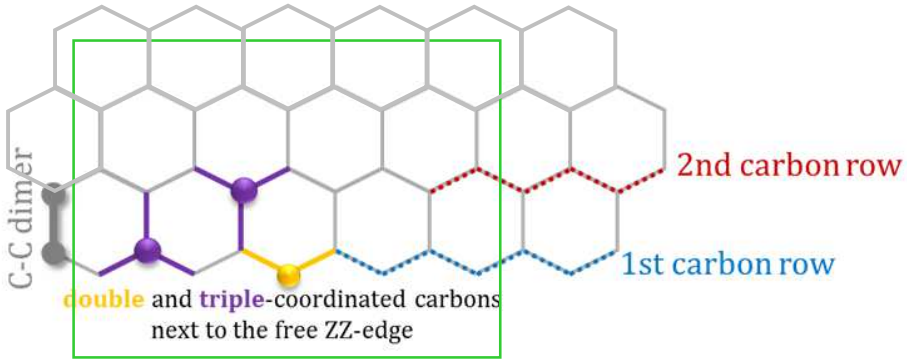

Figure 2. Schematic illustration of double and triple-coordinated carbon atoms next to the free ZZ edge. 1st and 2nd carbon rows, as well as C-C dimers, are defined along the GNR edges. The green zone represents the restricted area bombarded by H radicals (zone 1).

The simulation reported here analyses how a small area of the GNR edge (zone 1) is modified under cumulative H radicals bombardment at 800K. As illustrated in figure 2, zone 1 is centered on a free edge of the ZZ-GNR and contains only 27 carbon atoms. We define and number 2 specific carbon rows next to the edge: C atoms belonging to the 1st carbon row can be double-coordinated (5 atoms in zone 1) or triple-coordinated (4 atoms in zone 1), while all C atoms belonging to the 2nd carbon row are triple-coordinated. Partial or full removal of the 1st carbon row indicates that the GNR is etched from the edges. In the following, we also refer to so-called "C-C dimers" which correspond to pairs of 2 bonded C atoms from the 1st and 2nd rows (figure 2). Exposing such a small area to H impacts means that, ultimately, only 7 carbon atoms can be removed/etched from the 1st carbon row and edge effects may influence the etching process. However, our goal here is not to retrieve quantitatively the measured etching rates but to understand the basic mechanisms involved in the etching process by performing statistics over many impacts on a small zone of the surface.

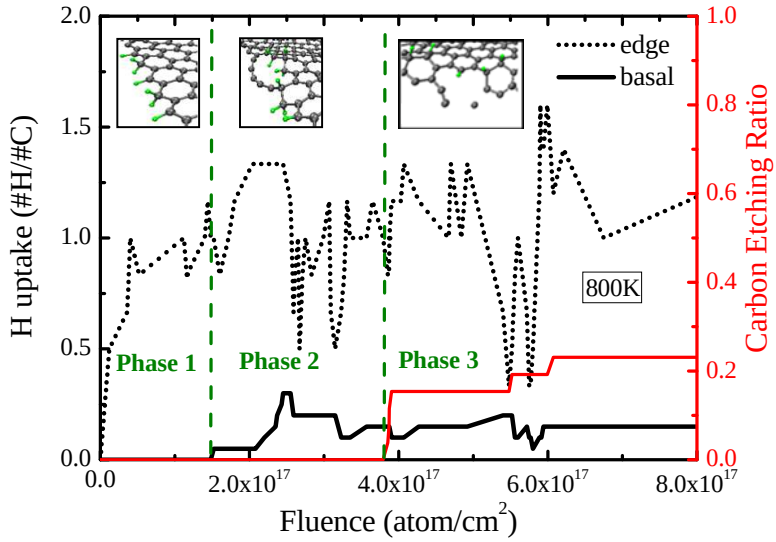

Figure 3. Hydrogenation of the GNR cell (zone 1) as function of the H fluence for E_R=T_S = 800K. Hydrogen uptake on the edges (double-coordinated C atoms) and on the basal plane (triple-coordinated C atoms) is shown with dotted and solid black lines respectively. The red curve represents the carbon etching ratio.

Figure 3 illustrates how the hydrogenation and the etching of the GNR (zone 1) proceeds as a function of the fluence of H plasma radicals at $E_R = T_S = 800$K. Here we consider separately the hydrogenation rates of the GNR edges (H uptake on double-coordinated C atoms) and of the GNR basal plane (H uptake on triple-coordinated C atoms). Rate values are calculated as the total number of H chemisorbed on double- (or triple-) coordinated C atoms divided by the total number of such C atoms in the exposed area (zone 1). Figure 3 also shows the evolution of the carbon etching ratio EC, calculated as the ratio between the number of etched C atoms and the total number of C atoms in the exposed area: $EC = N^{C}_{etched} / N^{C}_{total}$. Given the defined area, the removal of the 1st carbon row is then equivalent to a carbon etching ratio $EC_1 \sim 0.25$. We observe that the etching mechanism of the ZZ-edge occurs in three phases. Once the edge C atoms (double-coordinated) are fully hydrogenated (Phase 1), the inner C atoms next to the edge (triple-coordinated) also start to be hydrogenated which leads to the unzipping (local C-C dimers bond breaking) of the 1st carbon row (Phase 2). Then, the rupture of the unzipped/suspended carbon

chain induces the sputtering of its C atoms (Phase 3). Interestingly, the full mechanism of carbon etching from the ZZ-GNR edge does not require any volatile hydrocarbon product formation. In the following paragraph, all three phases are discussed in details.

a. Phase 1: Free edges hydrogenation

When exposing the virgin GNR to H radicals bombardment, figure 3 shows that H atoms first chemically attack the free edges while no chemisorption occurs on the basal plane. This was expected since, as previously reported[28], H chemisorption is barrierless on ZZ- and AC-GNR edges (unsaturated dangling bonds) while H atoms must overcome a 0.4-0.6 eV potential barrier to chemisorb on the graphene basal plane. This barrier is expected to decrease when the surface temperature increases[28]; however, it was shown to remain on the order of a few tenth of eV, which is high enough to prevent chemisorption of H atoms with E_R between 300K (~0.026eV) and 1000K (~0.086eV). Hence, there is initially no C-H bond formation on the triple-coordinated C atoms of the basal plane. The edge uptake H_{upt}^{edge} increases with the H fluence and reaches rapidly a quasi-steady state value. It oscillates between 0.8 and 1, indicating that H desorption from the edges also takes place, but that the H adsorption rate prevails over its desorption rate in these temperature conditions. As soon as the GNR edge is saturated with C-H bonds, the formation of CH_2 groups on the C edge atoms starts to be observed ($H_{upt}^{edge} > 1$ for a fluence ~1.5×10^{17}atom/cm^2). The formation of a significant density of CH_2 groups on the edges initiates Phase 2: the hydrogenation of the basal plane close to the edges.

Previous studies of elementary H/graphene interaction processes showed that the presence of one or more H adsorbates on the graphene surface strongly influences subsequent H adsorption and promotes the formation of energetically favorable H pairs[28]. In order to

understand the energetics of H chemisorption on/close to the edges, we calculated dynamically the potential energy barriers felt by an H atom impinging in the vicinity of one (or more) H atoms already chemisorbed on a GNR-edge at 0K. Results of these calculations are presented in figure 4 and show the energies required for H chemisorption on specific sites (in red) given specific surface configurations (in green). Interestingly, figure 4 suggests that the formation of a CH_2 group from an existing CH group requires an H impact with an energy $E_R \geq 0.5$ eV; it should therefore only very rarely observed at 800K since $E_R \sim 0.07$eV. However, hydrogenation at 800 K is characterized by strong thermal vibrations and a significant bending of the hydrogenated edges, both of which may significantly decrease the energy barrier for CH_2 formation compared to the 0K case. As expected, figure 4 also shows that the energy required for additional H chemisorption on the 1st and 2nd carbon rows depends strongly on the local atomic environment. In some configurations, the probability of C-H bond formation on triple-coordinated C atoms in the basal plane can become high. For example, when two CH_2 groups are located next to each other on the edge, H chemisorption on the inner C atom (1st row) can take place with only 0.1 eV at 0K. Such a mechanism is thus expected to be almost barrierless at 800 K and possible even with 0.07 eV H radicals. Therefore, as the hydrogen uptake on the edges (double-coordinated C) increases, the density of CH_2 groups rises, initiating the hydrogenation of triple-coordinated C atoms in the basal plane and Phase 2.

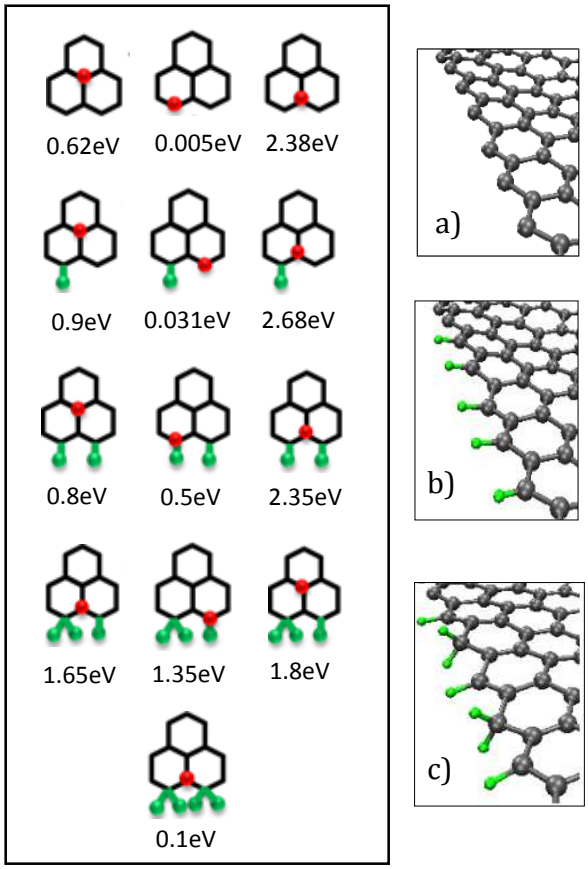

Figure 4. (Left) Energy required for H chemisorption on double- and triple- coordinated C atoms on the near-edge region. The schematics show the energy required for an H atom to chemisorb on the 1st and 2nd carbon row depending on the initial surface configuration (hydrogenation). Calculations are done for T_S = 0 K but all atoms are allowed to relax when interacting with the incident H. In each case, H atoms already chemisorbed are in green and below is indicated the energy required to chemisorb an extra H atom (in red) at a given position. (Right) Snapshots of the MD cell illustrating the evolution of the edge hydrogenation during Phase 1.

b. Phase 2: Inner C atoms hydrogenation and unzipping of edge C atoms

At the beginning of Phase 2, the hydrogenation of the GNR basal plane (H uptake on triple-coordinated C atoms) increases rapidly and reaches its maximum at a fluence of ~2.5×10^{17}atom/cm^2 (figure 3). Inner C atoms from the 1st and 2nd carbon rows start to be hydrogenated, which requires a local sp^2-sp^3 rehybridization resulting in structural changes of the GNR[28] surface and distorting its edges. As shown in figures 5a and 5b, C-H bond formation on these sites creates mechanical stress which distorts the honeycomb lattice and facilitates additional chemisorption of thermal H atoms on the 1st and 2nd carbon rows. The full hydrogenation of C-C dimers next to the edge (figure 5b and 5d) then induces a slight increase in

the C-C dimers bond length and the subsequent breaking of these dimers (figure 5c and 5e). To illustrate it, the evolution of the C-C dimer bond length in figures 5a)-c) is shown as function of the H fluence in Figure 6. Initially, the average C-C dimer bond length is equal to 1.42 Å, which matches the equilibrium bond length in the graphene honeycomb lattice (sp^2). As H atoms hydrogenate successively the two C atoms of the dimer, the C-C dimer bond is stretched due to the pair-rehybridization of the C atoms (sp^2 to sp^3) and its length increases up to 1.6 Å (figure 5b). This mechanical stress, further enhanced by thermal vibrations of the GNR edge, leads rapidly to the rupture of the C-C dimer bond (figure 5c). This *unzipping* process is caused by the distortion of the surface combined with the thermal vibrations of the lattice; it does not necessarily require additional H bombardment but occurs much faster if the area keeps being continuously bombarded. The consequence of multiple and adjacent C-C dimer bonds breaking (figure 5) is the formation of a suspended linear chain of C atoms on the GNR edge (figure 5f). This mechanism is called *unzipping* because as discussed later, it will propagate along the edge, thus separating the 1st and 2nd carbon rows like a zip. The creation of suspended unzipped C chains eventually leads to the last step of the etching process: chain breaking and carbon sputtering (i.e. etching).

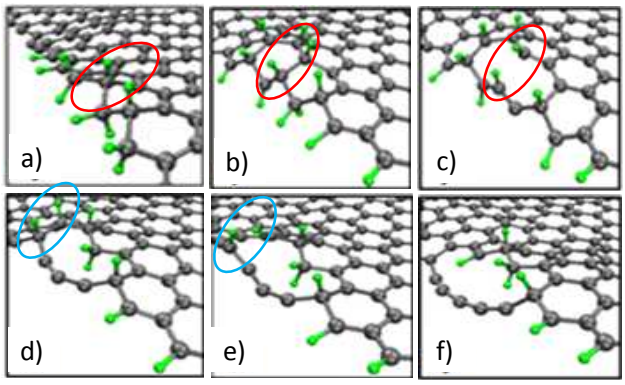

Figure 5. MD snapshots illustrating the series of mechanisms leading to the unzipping of the 1st carbon row in Phase 2. After hydrogenation of edge C atoms in Phase 1, inner C atoms next to the edge (triple-coordinated) start to be hydrogenated. It induces a slight increase in the C-C dimers bond length and the subsequent rupture of these dimers.

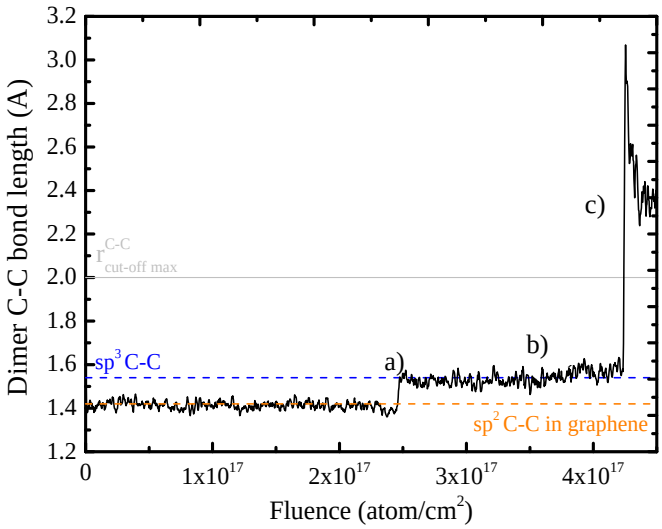

Figure 6. Bond length of a C-C dimer located next to the GNR edge as a function of the H fluence. The a)-c) letters refer to the snapshots presented in Figure 5.

c. Phase 3: Rupture of suspended C chains and C atoms sputtering

After being unzipped, the suspended linear C chains are weakened by the continuous H bombardment of the unzipped area and its surroundings. When H atoms impinge on the GNR close enough to (or on) an unzipped C chain, they deposit small amounts of energy in the system which enhance the amplitude of the C-C bonds vibrations in the unzipped chain. As a result, the suspended C chain - which already experiences significant bending and stretching - can eventually rupture from one side, leaving behind an unstable dangling chain of C atoms (figure 7a-b). The energy released by this 1st C-C bond rupture weakens the chain and initiates a series/cascade of sputtering events: all C atoms from the broken chain are sputtered one by one in the next few femtoseconds (figure 7c-d-e). Such a mechanism involves H bombardment and local energy deposition close enough to (or on) the suspended carbon chain. Sometimes, suspended C chains rupture and carbon sputtering also appear in conjunction with the absorption/desorption of H atoms next to (or on) the suspended C chain, or with the formation of CH_2 groups facing the unzipped C atoms (figure 7f-j). Indeed, such reactions inevitably induce

mechanical stress (or surface reconstruction) in the system, which facilitates the rupture of C-C bonds in the suspended C chain. Finally, as illustrated in figure 7k-o, the energy released by two simultaneous reactions (e.g. the rupture of a hydrogenated C-C dimer combined with an H desorption from the dimer) may also initiate the direct sputtering of a single C atom, rapidly followed by the sputtering of its chain neighbors.

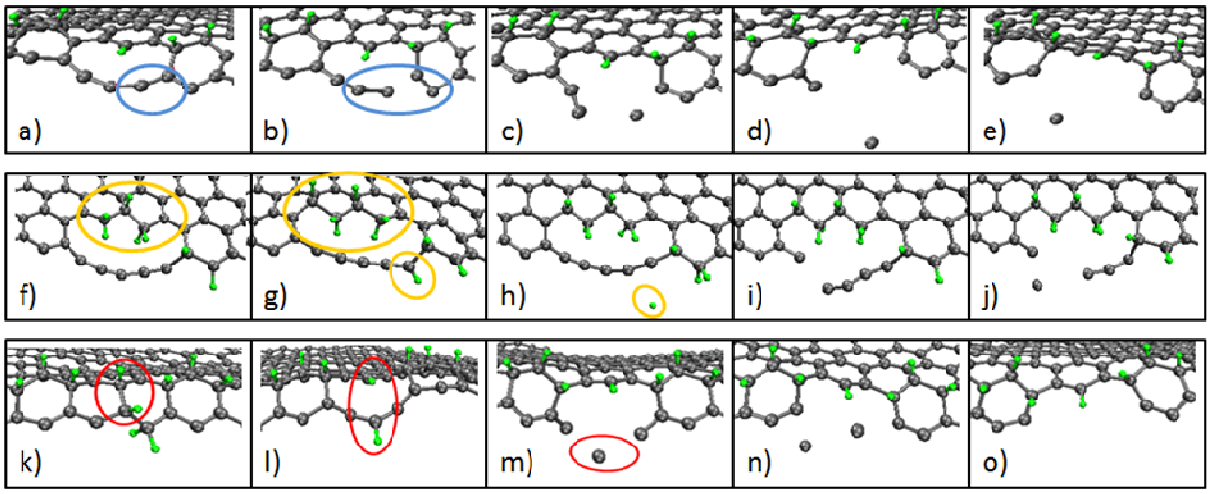

Figure 7. Series of snapshots illustrating 3 different mechanisms [a)-e), f)-j), k)-o)] which induce the rupture of a suspended C chain and carbon atom sputtering during Phase 3.

These examples show that carbon sputtering from unzipped/suspended C chains occurs due to a concerted mechanism, which requires high temperature, continuous hydrogenation and local mechanical stress induced in the system. The etching mechanism itself can be thought of as a sputtering process, since there is no need to form volatile etch products to remove C atoms from the GNR edges. As a matter of fact, the predominant etching by-products predicted in this study are single C atoms, with a smaller contribution from C_2 molecules. Therefore, contrary to expectations, no formation of volatile C_xH_y etch products is observed in this etching mechanism. This is an important conclusion since, as discussed later, this appears to be the root cause

explaining why the ribbon edges can be sharp-cut (without LER generation) rather than being 'nibbled' by H atoms as is the case in typical plasma etching processes.

Results found in the literature support our numerical predictions[33-36]. Chuvilin et al. reported TEM observations of graphene nanoribbons transformation to single carbon chains – an extreme lateral etching example induced by electron beam irradiation – in various configurations such as graphene bridges or between adsorbates[33]. Like in our study, they also observed the formation of singe carbon chains loops (unzipped) at the open edges of graphene sheets[33]. The unzipping mechanism was also observed experimentally in reactions between single-walled carbon nanotubes (SWNTs) and hydrogen gas. Talyzin et al. reported the unzipping of SWNTs into graphene nanoribbons as a result of hydrogenation at 400-550 °C[34]. John et al. also revealed the sequential electrochemical unzipping of SWNTs to graphene ribbons by *in situ* Raman spectroscopy and imaging[35]. This CNTs unzipping process was also analyzed through MD simulations using the reactive force field ReaxFF[36]. Dos Santos et al. reported that the unzipping process, which is responsible for CNTs opening, was due to the generation of local stress in the CNT[36]. All these groups concluded that almost perfectly linear cuts could be achieved in CNTs through the unzipping process, which suggests that a similar process can be suitable for cutting GNR edges. Reconstruction and evaporation of C atoms at the edges of ZZ-GNRs were also investigated through MD and DFT calculations[36]. At very high temperature (~3000 K), carbon atoms were found to evaporate (as single atoms) in a row-by-row fashion from the outermost zigzag edge region, with formation of linear carbon chains[36]. Finally, Jin et al. realized experimentally stable and rigid carbon atomic chains, by removing C atoms row-by-row from graphene through controlled energetic electron irradiation inside a TEM[37]. Like in our study, they report that a surface atom sputtering mechanism should dominate the thinning process,

which would be initiated by removing the double-coordinated C atoms at the two edges of the GNR and followed by the further sputtering of the adjacent C atoms[37].

2. Influence of the substrate temperature

In this subsection, MD calculations similar to those discussed in section III.A are performed for varying graphene substrate temperatures T_S (300K, 600K, 1000K). The goal of this study is to understand how T_S modifies the etching mechanism of ZZ-GNRs in downstream H_2 plasmas, and to provide a possible explanation for the temperature dependence of the etch rate observed experimentally (peaks at 800K and decrease for lower or higher substrate temperatures)[22,24,25]. Figure 8 illustrates how the hydrogenation and the etching of the GNR (zone 1) proceed as function of the H fluence for various surface temperatures T_S and for H radical energies E_R=T_S. Here again we present separately the hydrogenation rates of the GNR edges (H uptake on double-coordinated C atoms) and of the GNR basal plane (H uptake on triple-coordinated C atoms), as well as the carbon etching ratio. We observe that free edge hydrogenation takes place initially for all substrate temperatures. At room temperature (300K), saturation of edge C atoms (double-coordinated) leads mostly to single C-H bonds formation with very rare CH_2 group contributions. Figure 8a) also shows that hydrogenation of the basal plane is impossible because thermal H atoms (~0.026eV) do not have sufficient energy to chemisorb on triple-coordinated carbons[28]. Therefore, at room temperature, the required surface conditions to generate unzipping events (i.e. edge and near-edge H functionalization) are not reached and no etching is observed (the edge H uptake curve reaches a steady state). At 600K, hydrogenation of the GNR basal plane (H uptake on triple-coordinated C atoms) starts after a fluence of ~1.41×10^{17} atom/cm^2, i.e. as rapidly as at 800K (see figure 3). However, the inability of H atoms to bind on the C-C dimers configurations as fast as they do at 800K, slows down significantly the hydrogenation of the

inner C atoms (Phase 2). As a consequence, the fluence needed to initiate etching is ~7 times higher at 600K ($2.8x10^{18}$ atom/cm^2) than at 800K ($3.8x10^{17}$ atom/cm^2). This is partly attributed to the fact that at 600K, thermal vibrations and bending of the GNR hydrogenated edges do not reduce the surface potential barriers as strongly as at 800K. The H radicals energy is also smaller at 600K (E_R=0.052 eV) than at 800K (E_R=0.069 eV), which does not favor C-H bonds formation either. Although Phase 2 is slowed down at 600K compared to 800K, figure 8b shows that once etching starts (Phase 3), the basal plane hydrogenation remains high and the carbon etching ratio keeps increasing, indicating that etching is finally taking place. At higher temperature (1000K), the H uptake on the edges (double-coordinated C atoms) oscillates strongly and remains below 1 for fluences smaller than $4x10^{17}$atom/cm^2, indicating a competition between adsorption and spontaneous thermal desorption of H atoms on the free edges. This slows down significantly Phase 1, which lasts ~4 times longer than at 600K or 800K. Once the edge C atoms are fully hydrogenated ($H_{upt}^{edge} > 1$), hydrogenation of the basal plane increases rapidly with the H dose. This is due to strong thermal vibrations and to the higher energy of H radicals (E_R= 0.086eV) at 1000K, which lead to a higher probability of H chemisorption on the inner C atoms (2nd carbon row). As a consequence, Phase 2 is shorter than at 600K and carbon sputtering starts for a fluence ~$8x10^{17}$atom/cm^2, i.e. twice as long than at 800K but 3 times sooner than at 600K.

Even if our results are deduced from only a relatively restricted bombardment area (zone 1), interesting tendencies can be seen by comparing the evolution of the carbon etching ratio for temperatures T_S >300K. First, there is an H dose threshold (delay) to initiate etching, which depends on temperature (it is significantly higher at 600 K) and is due to the temperature dependence of the GNR hydrogenation rate in Phase 1 and Phase 2. However, since the equivalent timescale of fluences presented in figure 8 would be roughly about a second in real

plasma discharges, this delay should be negligible in processes which last many minutes. Furthermore, by looking at the carbon etching yields (#C removed per incident H) for the three temperatures, the lateral etching of the GNR appears to be faster at 800K than at 1000K or 600K, in qualitative agreement with experiments. In order to provide calculations for a more realistic case, the following section presents the results obtained when a larger area is cumulatively bombarded and hydrogenated at 800K.

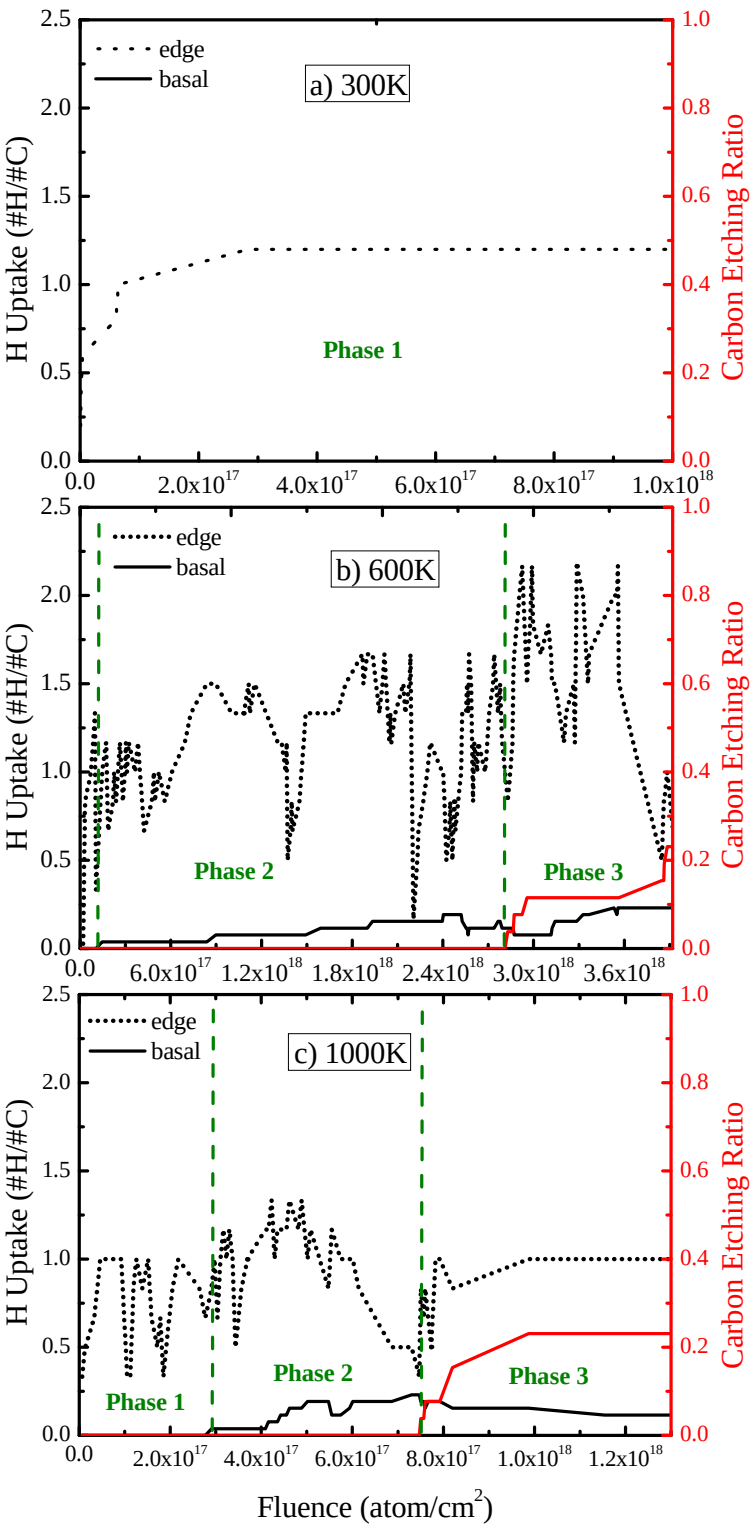

Figure 8. Hydrogenation of the GNR cell (zone 1) as function of the H fluence for E_R=T_S = a) 300K, b) 600K and c) 1000K. Hydrogen uptake on the edges (double-coordinated C atoms) and on the basal plane (triple-coordinated C atoms) is shown with dotted and solid black lines respectively. The red curve represents the carbon etching ratio.

B. Full ZZ-GNR trimming at T_S = 800K

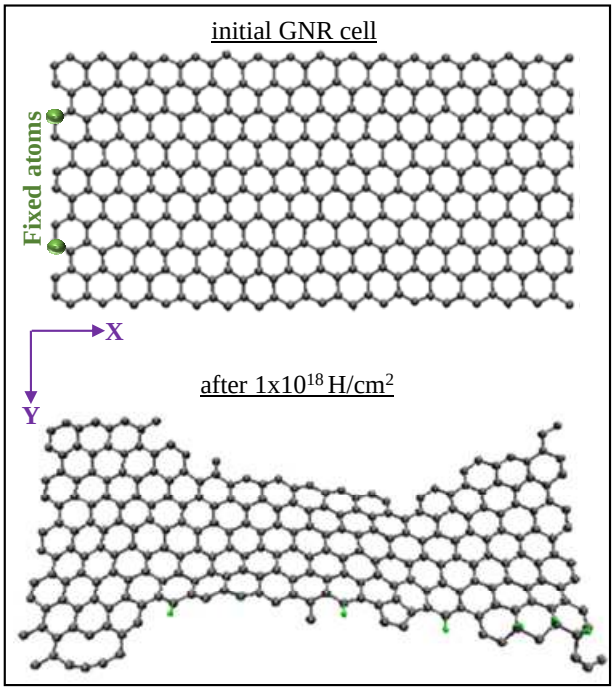

Figure 9. MD snapshots showing the evolution of the full GNR cell at 800K after an H fluence of $1x10^{18}$atom/cm^2.

In this section, a larger bombardment area – called zone 2 – is selected to study the propagation of the etch front and the trimming of the full GNR at 800K (red zone in figure 1). In this case again, only the free edges and a few adjacent carbon rows from the basal plane (3 along each free ZZ edge) are exposed to plasma radicals, i.e. those that are susceptible to react; the remainder of the cell is simulated but not bombarded. Figure 9 shows the evolution of the full GNR cell before and after an H fluence of $1x10^{18}$atoms/cm^2. We observe that almost two entire carbon rows were removed from the free GNR edges, which indicates that lateral etching takes place. One should note that the structure distortion and absence of etching near the extremities of the ribbon are only due to numerical edge effects. Indeed, as explained in section II, periodic boundary conditions are imposed along the Ox axis (to mimic a semi-infinite ribbon) and two

carbon atoms are maintained fixed on the periodic edges to anchor the graphene surface during H bombardment. Since these two fixed C atoms prevent both extremities of the GNR to behave the same way as its middle part, only the middle part of the ribbon should be considered here.

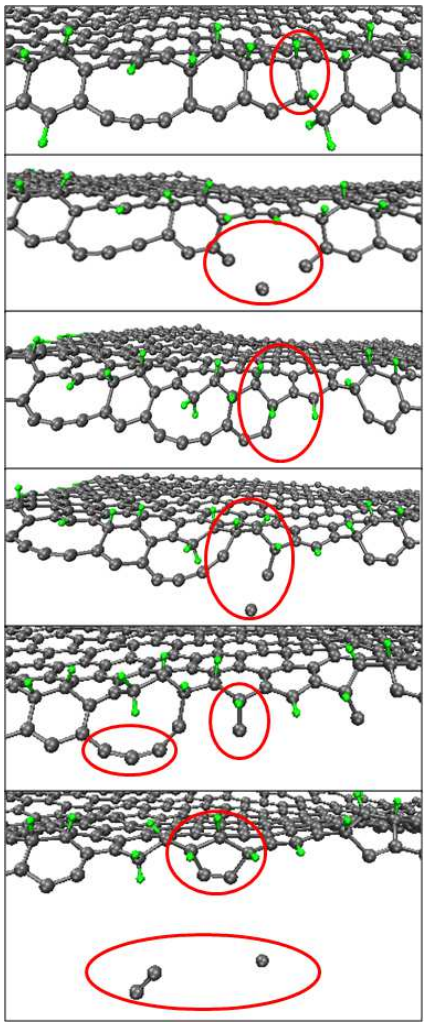

Figure 10. MD snapshots illustrating the propagation/cascade of unzipping and sputtering events along the GNR free edge at 800K.

Although numerical edge effects are inevitable for a finite computational domain and worsen as the cell size is reduced, all trends and conclusions drawn from the fundamental study carried out on zone 1 (see section III.A.1) are confirmed by this study on zone 2. In particular, if one excludes edge effects, no significant edge roughness (LER) is generated in the middle part of

the GNR cell during its lateral etching. This is a remarkable result but the reasons for this might be more complex than it was suggested earlier. Indeed, one could expect from results on zone 1 that the lateral etching of ZZ-GNRs could proceed row-by-row (i.e. by removing, one-by-one, one entire row of C atoms after unzipping it). Instead, we observe that lateral etching proceeds through a cascade of unzipping/sputtering events which propagates along the GNR edge, as illustrated in figure 10. In fact, unzipping a full carbon row is difficult because the hydrogenation of near-edge C-C dimers takes place randomly along the GNR (due to random H impacts locations), and as soon as any C-C dimer is hydrogenated, unzipping occurs rapidly (and locally) without any further bombardment assistance. Since it is impossible to saturate all near-edge C-C dimers at once, it is thus impossible to unzip an entire carbon row. Instead, suspended carbon chains containing between 3 and 5 atoms will appear randomly along the edge. And as shown in figure 10, the subsequent rupture of these unzipped chains will cause the sputtering of their C atoms.

At first glance, one could think that this random zone-by-zone etching should lead to the generation of LER. Our MD simulations show it is not the case, because the etching mechanism proceeds through a sequential cascade of unzipping and sputtering events, which propagates along the edge only. This is a self-limited process, since the etching cannot propagate to the 2nd or 3rd carbon rows before the 1st carbon row is removed from most part of the cell. The root cause is that hydrogenation of the basal plane far from the edge is highly unlikely due to the absence of sufficient stress and bending (caused by surface reconstruction), which are needed to reduce the surface potential barriers. Therefore, only the near-edge region is hydrogenated enough to produce unzipping, which typically propagates like an avalanche: the stress generated by C sputtering from one chain often initiates the rupture of neighbor unzipped chains and C sputtering from these chains (figure 10). This explains why the etching process does not generate

LER on the GNR edges: even if C atoms are removed step-by-step along the row on the edges, a global trend of row-by-row etching is still observed. This suggests that the process can be controlled at the atomic scale, allowing a precise control of the final ribbon dimension, as reported in experiments[22-25]. Moreover, while typical plasma etching processes relying on volatile hydrocarbon products formation would likely lead to strong edge roughness, the proposed unzipping mechanism does not. As shown in figure 11, no hydrocarbon etching products were observed through our entire MD study. Instead, almost 80% of etched carbon left as single C atoms and about 20% as C_2 molecules.

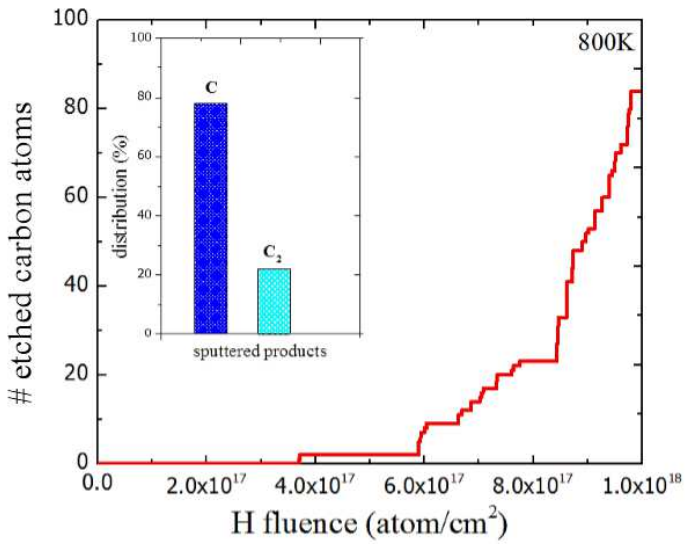

Figure 11. Carbon etching as function of the H fluence for the full GNR cell at 800K. Inset: Distribution of etching products.

IV. CONCLUSION

In this paper, we studied the lateral etching mechanism of suspended GNRs with free ZZ edges in downstream H_2 plasmas using Molecular Dynamics (MD) simulations. The influence of the substrate temperature on the etching mechanism was investigated and found to be in qualitative agreement with experiments. We proposed a new etching mechanism, which occurs in

three consecutive phases and requires a continuous exposure of the GNR to H atoms, as well as thermal vibrations of the graphene surface at high temperature (~800K). Phase 1 consists of the hydrogenation of the GNR edges and is possible because H atoms chemisorption is barrierless on free ZZ-edges (double-coordinated C atoms). Formation of both CH and CH_2 groups is observed on the edges during this phase. As a result, the surface potential barriers to H chemisorption on inner C atoms from the 1st and 2nd carbon rows can be reduced, allowing the hydrogenation of near-edge C atoms from the basal plane. An important step in the mechanism is the hydrogenation of C-C dimers from the 1st and 2nd carbon rows. Indeed, CH bond formation on these dimers creates mechanical stress between the two C atoms (due to local sp^2-to-sp^3 rehybridization and corresponding bond angle changes) and leads to the rupture of the C-C dimers bond, thus unzipping locally the 1st and 2nd carbon rows. At this point, H atoms previously bound to the edge C desorb, leaving behind chains of C with no attached H. This unzipping mechanism propagates randomly along the edges and creates linear carbon chains suspended along the edge of the ribbon (Phase 2). The suspended linear C chains are then weakened by the continuous H bombardment: H impacts bring additional energy in the system or mechanical stress by forming new CH bonds around the unzipped area. This sequence may result in the rupture of the suspended chains and the sputtering of their carbon atoms as C single atoms or C_2 molecules (Phase 3). All CH bonds formed on edge C atoms rupture before the C is sputtered since none of the sputtered C atoms was observed bound to H.

The original mechanisms evidenced by our MD study are supported by experimental results reported in the literature, especially in the field of carbon nanotubes (CNTs) where unzipping allows to transform CNTs into GNRs via a sharp and straight cutting of the nanotubes. The influence of substrate temperature on the fundamental etching mechanisms of ZZ-GNRs was also

investigated. Our analysis suggested the dominant mechanisms for understanding the temperature dependence of the etch rate observed experimentally (peaks at 800K and decreases for lower or higher substrate temperatures). This study demonstrates the capacity of classical MD to reproduce and explain the slow etching mechanisms of a 2D material - graphene - with quite good agreement with other theoretical and experimental works. We also underline that the proposed 3-phase mechanism is not intuitive since it occurs through a sputtering mechanism caused by mechanical stress (due to edge and near-edge H functionalization) and thermal vibrations, and not through hydrocarbon volatile products formation as in a typical plasma etching processes. H plays an important indirect role by forming CH bonds that alter the C atom hybridization, thus creating the mechanical stress that allows C-C bonds to break to form partially unzipped chains. But these crucially important CH bonds break before the unzipped chains rupture and before the C actually leaves the layer. This complex, sequential and counter-intuitive mechanism explains why the ribbon edges can be sharp-cut without generation of line-edge roughness (LER), as also observed experimentally.

Finally, computational edge effects appeared to be a non-negligible issue in our MD modelling of full ZZ-GNRs lateral etching. This numerical artefact arises from computationally necessary but unphysical C atom fixation on the periodic edges of the ribbon, which is required to anchor the graphene surface during H bombardment. In order to avoid these effects, none of the GNR atoms should be fixed in the simulation. For example, one could instead model bilayer GNRs (i.e. a GNR on top of an infinite graphene sheet) with no atom fixed on the top layer, or a GNR reported on top of a specific substrate (SiO2, Cu). This would however require the use/implementation of long-range attractive Van der Waals forces in the simulation, which are necessary to hold the sheets of graphene, or the GNR and the substrate, stacked together. These

forces were not included in the simulation results reported here, and further discussion of these forces is beyond the scope of the present paper. However, we note that our studies of bilayer GNRs including these forces show that the basic edge sputtering mechanism reported here is not affected by the lack of Van der Waals forces. By contrast, the presence of a different substrate material (SiO2, Cu) below the GNR could have an impact on the etching process, since H radicals could eventually chemisorb on the substrate surface (in absence of potential barrier) and migrate to the GNR edges, thus modifying the distribution of H atoms on the ribbon. The study of multilayer graphene interaction with H_2 plasma species, including Van der Waals forces, will be reported in a forthcoming paper.

ACKNOWLEDGMENTS

We are grateful to the Nanosciences Foundation of Grenoble, for the financial support of this work in the frame of the 2010 Chairs of Excellence Program. DBG acknowledges partial support from the US Department of Energy Office of Fusion Science.

REFERENCES

[1]Z Sun, DK James and JM Tour, J. Phys Chem. Lett. 2, 2425–2432 (2011)
[2]F Schwierz, Nature Publishing Group 5, 487–496 (2010)
[3]M Segal, Learning from silicon, Nature 1–2 (2012)
[4]LP Biró, P Nemes-Incze P & P Lambin, Nanoscale 4, 1824 (2012)
[5]Flores MZS, Autreto PAS, Legoas SB and Galvao DS, Nanotechnology 20 465704 (2009)
[6]Cheng S H, Zou K, Okino F et al, Phys. Rev. B 81 205435 (2010)
[7]Sofo J O, Chaudhari A S and Barber G D, Graphane: a two-dimensional hydrocarbon, Phys. Rev. B 75 153401 (2007)
[8]Ryu S, Han M Y, Maultzsch J, Heinz T F et al, Nano Lett. 8 4597–602 (2008)
[9]Elias D C, Nair R R, Mohiuddin T M G et al, Science 323 610 (2009)
[10]Robinson J T et al, Properties of fluorinated graphene films, Nano Lett. 10 3001–5 (2010)
[11]Leenaerts O, Peelaers H, Hernandez-Nieves A D et al, Phys. Rev. B 82 195436 (2010)
[12]Ci L et al, Nature Mater. **9**, 430–435 (2010)
[13]Son, YW, Cohen ML and Louie SG, Phys. Rev. Lett. **97**, 216803 (2006)

[14]Nakada K, Fujita M, Dresselhaus G and Dresselhaus MS, Phys. Rev. B 54 17954 (1996)
[15]J Cai, P Ruffieux, R Jaafar et al, Nature 466(7305), 470-473 (2010)
[16]PL Neumann et al, Nucl. Instr. and Methods in Physics Research B 282, 130–133 (2012)
[17]M. Han, B. Ozyilmaz, Y. Zhang and P. Kim, Phys. Rev. Lett. 98, 206805 (2007)
[18]C. Berger, Z. Song, X. Li et al, Science, 312, 1191–1196 (2006)
[19]L. A. Ponomarenko, F. Schedin, M. I. Katsnelson et al, Science, 320, 356–358 (2008)
[20]Z. Chen, Y. Lin, M. Rooks and P. Avouris, Phys. E., 40, 228–232 (2007)
[21]L J iao, L Xie and H Dai, Nano Research 5(4), 292-296 (2012)
[22]R Yang, L Zhang, Y Wang et al., Adv. Mater. 22, 4014-4019 (2010)
[23]X. Wang and H. Dai, Nat. Chem., 2, 661–665 (2010)
[24]Diankov et al, ACS Nano vol 7, 2, 1324–1332 (2013)
[25]Xie L, Jiao L and Dai H, J. Am.Chem. Soc. *132*, 14751–14753 (2010)
[26]J Tersoff, Phys. Rev. B 37, 6991 (1988)
[27]DW Brenner, OA Shenderova, JA Harrison et al, J. Phys.: Condens. Matter 2002, 14 (783)
[28]E Despiau-Pujo, AO Davydova, G Cunge et al, J. Appl. Phys. 113, 114302 (2013)
[29]HJC Berendsen et al, Journal of Chemical Physics 81, 8, 3684–3690 (1984)
[30]WC Swope, HC Andersen, PH Berens and KR Wilson, J. Chem. Phys. 76, 637 (1982)
[31]E Despiau-Pujo, P Chabert, J. Vac. Sci. Technol. A, 28, 1105-1110 (2010)
[32]P Brichon, E Despiau-Pujo, O Joubert, J. Vac. Sci. Technol. A, 32, 021301 (2014)
[33]A Chuvilin, JC Meyer, G Algara-Siller, U Kaiserew, New Journal of Physics 11 (2009) 083019
[34]AV Talyzin, S Luzan, IV Anoshkin et al, ACS Nano, 5(6), 5132-5140 (2011)
[35]RPB Dos Santos et al, Nanotechnology, 23, 465702 (2012)
[36]GD Lee, CZ Wang et al, Phys. Rev. B 81, 195419 (2010)
[37]C Jin, H Lan, L Peng et al, Phys. Rev. Lett. 102, 205501 (2009)